physica status solidi a
www.pss-a.com

Check for updates

Optical, Electrical, and Optoelectronic Characterization of Ti-Supersaturated Gallium Arsenide

Sari Algaidy, Daniel Caudevilla, Guillermo Godoy-Pérez, Rafael Benítez-Fernández, Francisco Pérez-Zenteno, Sebastián Duarte-Cano, Rodrigo García-Hernansanz, Enrique San Andrés, Eric García-Hemme, Javier Olea, Jan Siegel, José Gonzalo, David Pastor,* and Álvaro del Prado**

Herein, a detailed investigation on the properties of supersaturated gallium arsenide (GaAs) using Ti^+ implantation followed by nanosecond pulsed laser melting (PLM) is presented. The supersaturated samples are analyzed by means of electrical, optical, and optoelectronic characterization. The sheet resistance results obtained using van der Pauw configuration measurements do not show activation of the implanted Ti^+ in semi-insulating GaAs after PLM. Absorptance measurements show a sub-bandgap absorption (up to 6.5% for $\lambda = 1000$ nm) of the supersaturated GaAs:Ti and the just PLM-processed GaAs, with the same laser melting fluence used (0.50 J/cm^{-2}). The origin of this sub-bandgap absorption is analyzed. Optoelectronic measurements show a similar sub-bandgap photo-response related to the absorption analyzed. The photo-response measured below the bandgap originates from point defects introduced by the PLM process.

1. Introduction

Supersaturated semiconductors are of great interest in obtaining materials with advanced capabilities. By using nonequilibrium techniques, ion implantation of semiconductors with transition metals such as (Ti, Mn, Cr, etc.) followed by laser annealing, we can increase the material capabilities to absorb photons in the sub-bandgap region.[1] This increase would allow to fabricate improved photovoltaic devices and photodetectors.[2,3] It is well known that gallium arsenide (GaAs) is one of the most used III–V semiconductors for device fabrications. This is due to the natural capabilities of GaAs in absorbing photons, which is a direct consequence of having a direct bandgap in the band structure.

Many supersaturated systems based on well-known semiconductors, such as Si,[4] GaP,[5] Ge,[6] GaN,[7,8] and InP,[9] have demonstrated remarkable results for photovoltaic and infrared (IR) photodetection using ion implantation and followed by laser annealing. Beyond optoelectronic applications, supersaturating GaAs with suitable impurities, such as Mn and Fe, can produce ferromagnetic properties that can be implemented in spintronic technologies.[10,11]

According to *ab initio* calculations of the electronic band structures of Ga_nAs_mM and Ga_nP_mM compounds, Ti is identified as a candidate to produce an isolated partially filled band within the GaAs bandgap.[12] It has been calculated that the formation of this band by Ti occupying substitutional Ga sites in GaAs requires an increase of energy. However, this increase is smaller than the required for the formation of the Ga_nP_mTi compound[2] and supersaturated GaP:Ti with sub-bandgap photo-response has been achieved using the same ion implantation followed by pulsed laser melting (PLM) approach analyzed in this work.[5]

In a previously published paper,[13] we examined the structural characteristic of Ti-supersaturated GaAs using multiple characterization techniques. The results showed a successful recovery of the crystalline structure of the material after ion implantation.

In this article, we are aiming to obtain a sub-bandgap photo-response. We will examine the optical, electrical, and optoelectronics characteristics of Ti-supersaturated GaAs. The optical results show an increase in absorption of up to 6.5% with the

S. Algaidy
Instituto de Energía Solar
Universidad Politécnica de Madrid
E.T.S.I. Telecomunicación
Cuidad Universitaria, 28040 Madrid, Spain
E-mail: Sari.algaidy@alumnos.upm.es

D. Caudevilla, G. Godoy-Pérez, R. Benítez-Fernández, F. Pérez-Zenteno, S. Duarte-Cano, R. García-Hernansanz, E. San Andrés, E. García-Hemme, J. Olea, D. Pastor, Á. del Prado
Department Estructura de la Materia
Física Térmica y Electrónica, Fac. CC.Fisica, University Complutense de Madrid
28040 Madrid, Spain
E-mail: dpastor@ucm.es; adelprado@ucm.es

J. Siegel, J. Gonzalo
Laser Processing Group
Instituto de Óptica
IO-CSIC
Serrano 121, 28006 Madrid, Spain

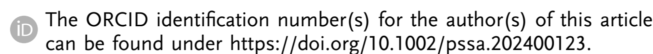
The ORCID identification number(s) for the author(s) of this article can be found under https://doi.org/10.1002/pssa.202400123.

© 2024 The Authors. physica status solidi (a) applications and materials science published by Wiley-VCH GmbH. This is an open access article under the terms of the Creative Commons Attribution License, which permits use, distribution and reproduction in any medium, provided the original work is properly cited.

DOI: 10.1002/pssa.202400123

18626319, 0, Downloaded from https://onlinelibrary.wiley.com/doi/10.1002/pssa.202400123 by Spanish Cochrane National Provision (Ministerio de Sanidad), Wiley Online Library on [21/11/2024]. See the Terms and Conditions (https://onlinelibrary.wiley.com/terms-and-conditions) on Wiley Online Library for rules of use; OA articles are governed by the applicable Creative Commons License

just PLM-processed sample and the Ti-implanted and PLM-processed sample, in the sub-bandgap region. This is also reflected in the results for the photo-response obtained in the optoelectronics characterization. However, no electrical activation of the Ti is observed. The results suggest that the PLM process itself can modify the properties of GaAs for sub-bandgap absorption with potential application in IR photodetection and photovoltaic devices.

2. Results and Discussion

TEM was used to analyze the structural properties. **Figure 1** shows the cross-sectional TEM images of the as-implanted sample, just PLM-processed sample, and the Ti-implanted and PLM-processed sample. For the as-implanted sample, an amorphous layer of approximately 45 nm is observed as a consequence of the ion-implantation process. For the just PLM-processed sample, no effect on the crystallinity of the GaAs was observed, neither the formation of any extended defect. However, a surface oxide layer about 5 nm thick was observed after the PLM. In the case of the amorphous Ti implanted layer that has been PLM processed, the crystallinity has been recovered. The oxygen presence in the surface layer is also observed. Some bubble-like structures related to regions with higher Ti concentration are also observed. A full description of the structural characterization of Ti-supersaturated GaAs has been previously described in the literature.[13]

Figure 2 shows the absorptance, obtained from the measured transmittance and reflectance for the GaAs reference, a sample processed by PLM at laser fluence of 0.50 J/cm^{-2} (GaAs + PLM), an implanted sample and subsequently processed by PLM at laser fluence of 0.50 J/cm^{-2} (GaAs:Ti + PLM), and an as-implanted sample (GaAs:Ti). The normalized transmittance and reflectance measurements can be found in Figure S4, Supporting Information, as well as in Figure 4, for the sub-bandgap region.

For all the samples, the expected steep absorption edge corresponding to the GaAs direct bandgap is observed. For energies above the bandgap (wavelengths below 872 nm), transmittance becomes effectively 0, as a consequence of all non-reflected light being absorbed (in other words, internal absorptance becomes 1) and the measured absorptance corresponds directly to $1-R$. In this range, it is not possible to obtain information from these measurements of the absorption coefficient, since all light is absorbed within a thickness much lower than the 325 μm substrate thickness. The observed decrease of A is directly related to the increase of R. For the reference substrate and the PLM-processed samples, a slight increase of absorptance with respect to the theoretical value of 0 is observed starting around $\lambda = 1500$ nm (not shown here). We attribute this small absorption to point defects which are present even in the reference substrate.

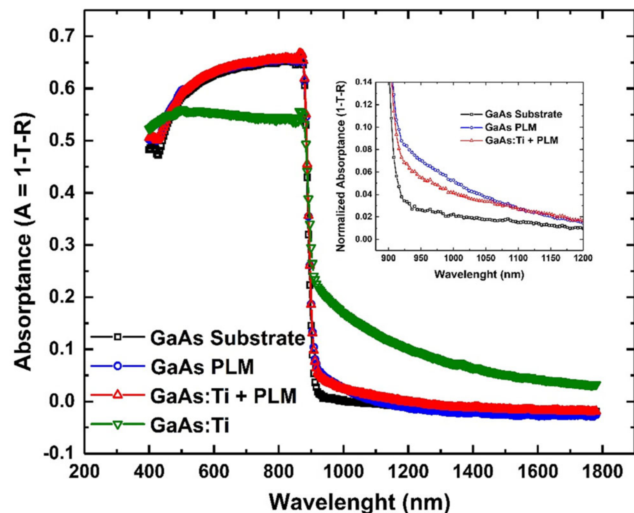

Figure 2. Absorptance of the GaAs reference, GaAs:Ti, GaAs + PLM, and GaAs:Ti + PLM processed at 0.50 J/cm^{-2}.

For both samples processed by PLM, a clear increase of the absorption with respect to the substrate is also observed extending into the immediate below bandgap region of the GaAs, with a maximum increase of absorptance of up to 6.5% for a wavelength of $\lambda = 950$ nm for the GaAs + PLM sample. Similar sub-bandgap absorption tails have been previously reported for laser-processed GaAs[14] and weakly damaged ion implanted GaAs[15–17] and attributed to the formation of point defects or clusters of point defects during the PLM or ion-implantation process. Since this absorption is observed for both GaAs + PLM and GaAs:Ti + PLM samples, we conclude that it is related to defects

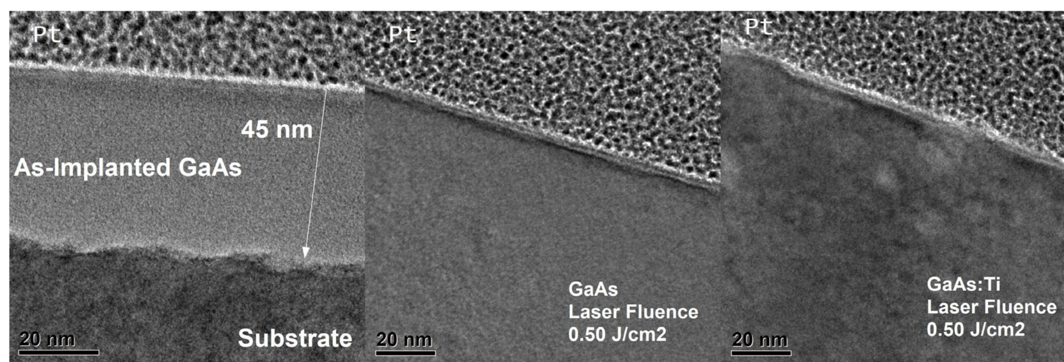

Figure 1. TEM images of as-implanted GaAs with Ti (left), GaAs + PLM at laser fluence of 0.50 J/cm^{-2} (middle), and GaAs:Ti + PLM at laser fluence of 0.50 J/cm^{-2} (right).

© 2024 The Authors. physica status solidi (a) applications and materials science published by Wiley-VCH GmbH

induced by the PLM process rather than to the incorporation of Ti providing optically active states. Defects are certainly induced during the Ti implantation, but the sub-bandgap absorption of the GaAs:Ti + PLM sample is not higher than for the GaAs + PLM sample, suggesting that the effect of the PLM process is dominant.

The inset of Figure 2 shows a detail of the normalized absorptance in the below bandgap region, where the enhanced absorption is observed for the samples processed by PLM. The normalized data have been used for the following absorption coefficient calculations.

For the as-implanted sample (GaAs:Ti), a much stronger below bandgap absorptance is observed, extending up to the measured wavelength limit $\lambda = 1780$ nm, with a significantly higher reflectance and lower transmittance. The increased reflectance suggests a significant change of the refractive index of the implanted amorphous layer with respect to the substrate. Strong sub-bandgap absorption, together with an increase of the refractive index, is characteristic of amorphous GaAs after ion implantation.[18] Therefore, the optical results for this sample are consistent with the TEM measurements previously shown. Given the amorphous structure of the implanted layer (as shown in Figure 1), roughness at the surface or at the interface with the substrate cannot be discarded (even though the sample remains specular to the eye). So, the measured absorptance could overestimate the actual absorptance because of a small fraction of the light being reflected and transmitted at dispersed directions. Yet, the increased reflectance with respect to the substrate makes it clear that the increased absorptance could not be simply attributed to dispersed reflected light not being collected.

To obtain the optical parameters of the processed layer, a two layers model for the sample with front and back air layers is used, following the method described by Maley.[19] The model is shown in **Figure 3**, together with the parameter notation for each layer. The top layer (layer 2) is the processed layer (just PLM, Ti implantation + PLM or as implanted). For substrate calculations, this layer is not included in the model. Therefore, following the incoherent limit, the transmittance and reflectance for the substrate are given by[19]

$$R_{\text{GaAs}} = |r_{13}|^2 + \frac{|t_{13}|^2|t_{31}|^2|r_{34}|^2 e^{-2\alpha_3 t_3}}{1 - |r_{31}|^2|r_{34}|^2 e^{-2\alpha_3 t_3}} \tag{1}$$

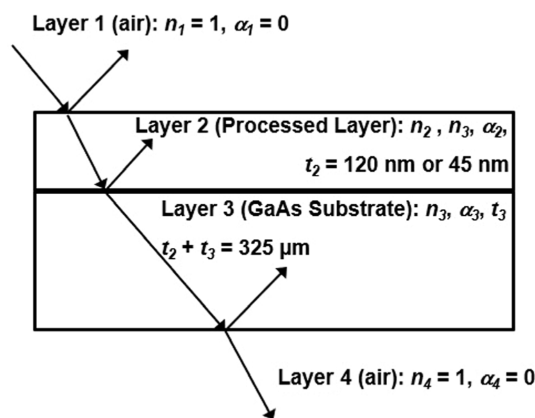

Figure 3. Two-layer model for optical analysis.

$$T_{\text{GaAs}} = |t_{13}|^2|t_{34}|^2 \frac{e^{-\alpha_3 t_3}}{1 - |r_{31}|^2|r_{34}|^2 e^{-2\alpha_3 t_3}} \tag{2}$$

The Fresnel's coefficients in Equation (1) and (2) are given by

$$r_{ij} = \frac{N_i - N_j}{N_i + N_j}; t_{ij} = \frac{2N_i}{N_i + N_j} \tag{3}$$

N_i is the complex refractive index of layer i: $N_i = n_i - ik_i$.

Equation (1) and (2) are fitted to the experimental normalized transmittance and reflectance of the substrate. For the real part of the refractive index, a Sellmeier equation of the type given by Skauli et al.[20] is used:

$$n(\lambda)^2 = g_0 + \frac{g_1}{\lambda_1^{-2} - \lambda^{-2}} + \frac{g_2}{\lambda_2^{-2} - \lambda^{-2}} + \frac{g_3}{\lambda_3^{-2} - \lambda^{-2}} \tag{4}$$

The fitting parameters are the coefficients g_0, g_1, g_2, g_3, λ_1, λ_2, λ_3, and the exponential term $e^{-\alpha_3 t_3}$. The thickness is fixed to the value given by the manufacturer ($t_3 = 325$ µm). The used fitting range is from $\lambda = 864$ nm to $\lambda = 1780$ nm. The resulting values are used as the layer three parameters for the calculations of the parameters of the processed layer, according to the two layers model of Figure 3.

It is important to point that, once the bandgap energy is exceeded ($\lambda < 872$ nm) and α_3 reaches a sufficiently high value, the term $e^{-\alpha_3 t_3}$ becomes effectively 0 and it is not possible to obtain information about α_3 beyond this range. For the range $\lambda \geq 872$ nm, the fitting parameter $e^{-\alpha_3 t_3}$ does provide information of the absorption coefficient and therefore the imaginary part of the refractive index.

Concerning the GaAs + PLM and GaAs:Ti + PLM samples, if there was a difference in the refractive indexes of the processed layer and the substrate, multiple reflections would take place at this interface, and characteristic maxima and minima, depending on the thickness, would appear in both the reflectance and transmittance spectra. None of these features have been observed. In addition, for the wavelength range above the GaAs bandgap, no significant differences were observed for the reflectance spectra of the samples processed by PLM and the GaAs reference. In this aforementioned bandgap range, the transmittance drops to 0 due to total absorption of the signal by the substrate and the reflectance depends only on the refractive index of the top layer (layer 2) and possible multiple reflections in the interface between layers 2 and 3. Therefore, we have assumed that no significant changes take place in the refractive index of the processed layer with respect to the substrate and that the influence of these possible multiple reflections is negligible. Very small or negligible variations of the real part of the refractive index $\Delta n/n \leq 0.01$ have reported for defective crystalline GaAs.[18] This is also supported by the fact that the implantation profile is quite smooth after the PLM process. There is no abrupt change in the Ti concentration.[12] This means that $r_{23} \approx 0$ and $t_{23} \approx 1$. For our model, we have set the real part of the refractive index of layer 2 equal to the substrate value (layer 3). We considered the imaginary part of N_2 when computing t_{12}, t_{21}, r_{12}, and r_{21}. Yet, we will show later that its influence is also negligible. The assumption of neglecting the multiple reflections at the interface between layers 2 and 3 is further supported by the cross-sectional

© 2024 The Authors. physica status solidi (a) applications and materials science published by Wiley-VCH GmbH

18626319, 0, Downloaded from https://onlinelibrary.wiley.com/doi/10.1002/pssa.202400123 by Spanish Cochrane National Provision (Ministerio de Sanidad), Wiley Online Library on [21/11/2024]. See the Terms and Conditions (https://onlinelibrary.wiley.com/terms-and-conditions) on Wiley Online Library for rules of use; OA articles are governed by the applicable Creative Commons License

18626319, 0, Downloaded from https://onlinelibrary.wiley.com/doi/10.1002/pssa.202400123 by Spanish Cochrane National Provision (Ministerio de Sanidad), Wiley Online Library on [21/11/2024]. See the Terms and Conditions (https://onlinelibrary.wiley.com/terms-and-conditions) on Wiley Online Library for rules of use; OA articles are governed by the applicable Creative Commons License

TEM images in Figure 1, in which no such interface is distinguished for the PLM and GaAs + PLM samples. This approach was also previously used when analyzing absorption in Si hyperdoped with Ti[21] and has also been followed to analyze weakly damaged ion-implanted GaAs.[17]

Following this approach, the reflectance and transmittance of the samples processed by PLM are given by

$$R_{\mathrm{GaAs+PLM}} = |r_{12}|^2 + \frac{|t_{12}|^2|t_{21}|^2|r_{34}|^2 e^{-2\alpha_2 t_2} e^{-2\alpha_3 t_3}}{1-|r_{21}|^2|r_{34}|^2 e^{-2\alpha_2 t_2} e^{-2\alpha_3 t_3}} \tag{5}$$

$$T_{\mathrm{GaAs+PLM}} = |t_{12}|^2|t_{34}|^2 \frac{e^{-\alpha_2 t_2} e^{-\alpha_3 t_3}}{1-|r_{21}|^2|r_{34}|^2 e^{-2\alpha_2 t_2} e^{-2\alpha_3 t_3}} \tag{6}$$

The fitting range for these samples was from 1620 nm (for higher wavelengths no absorptance was observed) to 864 nm. The fitting parameter is the exponential term $e^{-\alpha_2 t_2}$. It must be noted that the absorption coefficient in the processed layer may not be constant as a function of depth. So, $\alpha_2 t_2$ corresponds to the integrated absorption coefficient over the processed layer: $\alpha_2 t_2 = \int_0^{t_2} \alpha(z) dz$. The substrate parameters are fixed to the values obtained from the analysis of the GaAs reference. The thickness of layer 2 has been set to $t_2 = 120$ nm. This value is obtained from simulations of the melted depth of the sample using the software laser-induced melting predictions (please check Figure S5, Supporting Information). The thickness is used to compute α_2 and k_2. While it does affect the actual value of the absorption coefficient α_2, its influence in the actual fitting is negligible, because k_2 is too small to have a significant influence on the Fresnel's coefficients t_{12}, t_{21}, r_{12}, and r_{21}. Given the much higher thickness of the substrate compared to the thickness of the processed layer, once the bandgap absorption edge starts, the influence of the substrate absorption is very high and any small dispersion (in the order of the resolution of the equipment) in the measured transmittance of the processed samples with respect to the substrate results in an inaccurate computing of α_2. We have observed this limitation for wavelengths below 890 nm. It must also be noted that roughness is not being considered. Given the high crystalline quality of the PLM-processed samples observed by TEM, this possible source of error is not expected to be significant. The model could be refined to consider multiple reflections at the interface between the processed layer and the substrate (removing the assumption of $n_2 = n_3$). Another possibility would be to consider a graded refractive index-processed layer in which at the substrate interface $n_2 = n_3$ but with a different n_2 value at the surface for the purpose of computing r_{12}, r_{21}, t_{12}, and t_{21}. We have indeed tried these approaches for the GaAs + PLM sample and no better fittings in terms of total error were obtained (error is obtained as the sum of the absolute value of the difference between measured and calculated R and T over the whole fitting range).

For the GaAs:Ti sample, a clear interface is observed between the as-implanted layer and the substrate. Therefore, the two layers model is followed without any simplification. For the real part of the refractive index a Sellmeier equation of the type of Equation (4) was used, and the coefficients g_0, g_1, g_2, g_3, λ_1, λ_2, and λ_3 were fitting parameters, together with the exponential term $e^{-\alpha_2 t_2}$, instead of being fixed at the values obtained for the substrate. The thickness for the as-implanted layer was set to 45 nm according to the TEM results shown in Figure 1. We note that for this small thickness, no characteristic maxima and minima form multiple reflections at the interface with the substrate are observed in the analyzed range, although the shape of R and T is indeed influenced by these reflections.

The fitting results for all the processed samples are shown in **Figure 4**. A good fitting of the experimental results is obtained. For the GaAs:Ti sample, the obtained values of n_2 are nearly constant varying from $n_2 = 4.095$ at $\lambda = 1780$ nm to $n_2 = 4.106$ at $\lambda = 864$ nm. This represents a relative increase with respect to the substrate value: $\Delta n/n = 0.11$–0.22, depending on the wavelength, similar to the value reported in ref. [18].

Figure 5 shows the resulting exponential factor $\alpha_2 t_2$ (product of the absorption coefficient and layer thickness) for the processed layers of samples GaAs:Ti, GaAs + PLM, and Ga:As: Ti + PLM as a function of energy. An exponential dependency of $\alpha_2 t_2$ is observed for all the samples (especially clear for the GaAs:Ti sample, less clear for the GaAs:PLM sample), except for energies very close to 0.8 eV for the PLM-processed samples, where the absorption coefficient approaches 0, and for very high energies, where the GaAs absorption edge influences the absorption coefficient.[15] For energies below 0.93 eV ($\lambda > 1330$ nm), the absorptance in the PLM-processed layers is very small and the dispersion on the T and R measurements due to the spectrometer resolution affects the fitted results. For the GaAs:Ti sample, considering a thickness of the amorphous layer of 45 nm, very high values of the absorption coefficient α_2 ranging from 1.1×10^4 cm^{-1} at 0.7 eV to 1.1×10^5 cm^{-1} at 1.39 eV are obtained. These values are similar to the ones reported for N-implanted GaAs.[18] While these values are very high, the amorphous structure of the as-implanted layer will lead to a completely degraded mobility, not suitable for device applications requiring the collection of photogenerated carriers. For the PLM-processed layers, considering a 120 nm thickness for the processed layers, as explained earlier, values of the absorption coefficient α_2 in the 10^3 cm^{-1} range are obtained for energies above 1.12 eV, with values as high as 7×10^3 cm^{-1} for the highest energy analyzed (1.39 eV).

Figure 5 also shows the fitting of the GaAs:Ti and GaAs: Ti + PLM samples data to an equation of the type:

$$\alpha_2 t_2 = A e^{\frac{h\nu}{E_0}} \tag{7}$$

The chosen energy range for the fitting for the GaAs:Ti sample was from 0.697 to 1.37 eV (avoiding the last points influenced by the GaAs absorption edge, which show a different slope). For the PLM-processed samples, the initial energy was 0.925 eV (for which $\alpha_2 > 250$ cm^{-1} and the dispersion of the data is not too high). The obtained parameters for the GaAs:Ti sample were $\mathrm{Ln}A = -5.140 \pm 0.004$ eV^{-1} and $1/E_0 = 3.065 \pm 0.004$ eV^{-1}, with a regression parameter $r = 0.9998$, which yields $E_0 = 0.33$ eV. This value is higher than the reported by Wesch et al.[18] for amorphous GaAs (0.175 eV), but it is very similar to the saturation value (around 0.3 eV) reported by Zammit et al. for GaAs implanted with Si, once the mean energy per unit volume deposited by nuclear collision ($\overline{G}_n$) surpasses the threshold for amorphization of the GaAs.[15] An estimation of $\overline{G}_n$ for our samples as the implanted dose multiplied by the

© 2024 The Authors. physica status solidi (a) applications and materials science published by Wiley-VCH GmbH

18626319, 0, Downloaded from https://onlinelibrary.wiley.com/doi/10.1002/pssa.202400123 by Spanish Cochrane National Provision (Ministerio de Sanidad), Wiley Online Library on [21/11/2024]. See the Terms and Conditions (https://onlinelibrary.wiley.com/terms-and-conditions) on Wiley Online Library for rules of use; OA articles are governed by the applicable Creative Commons License

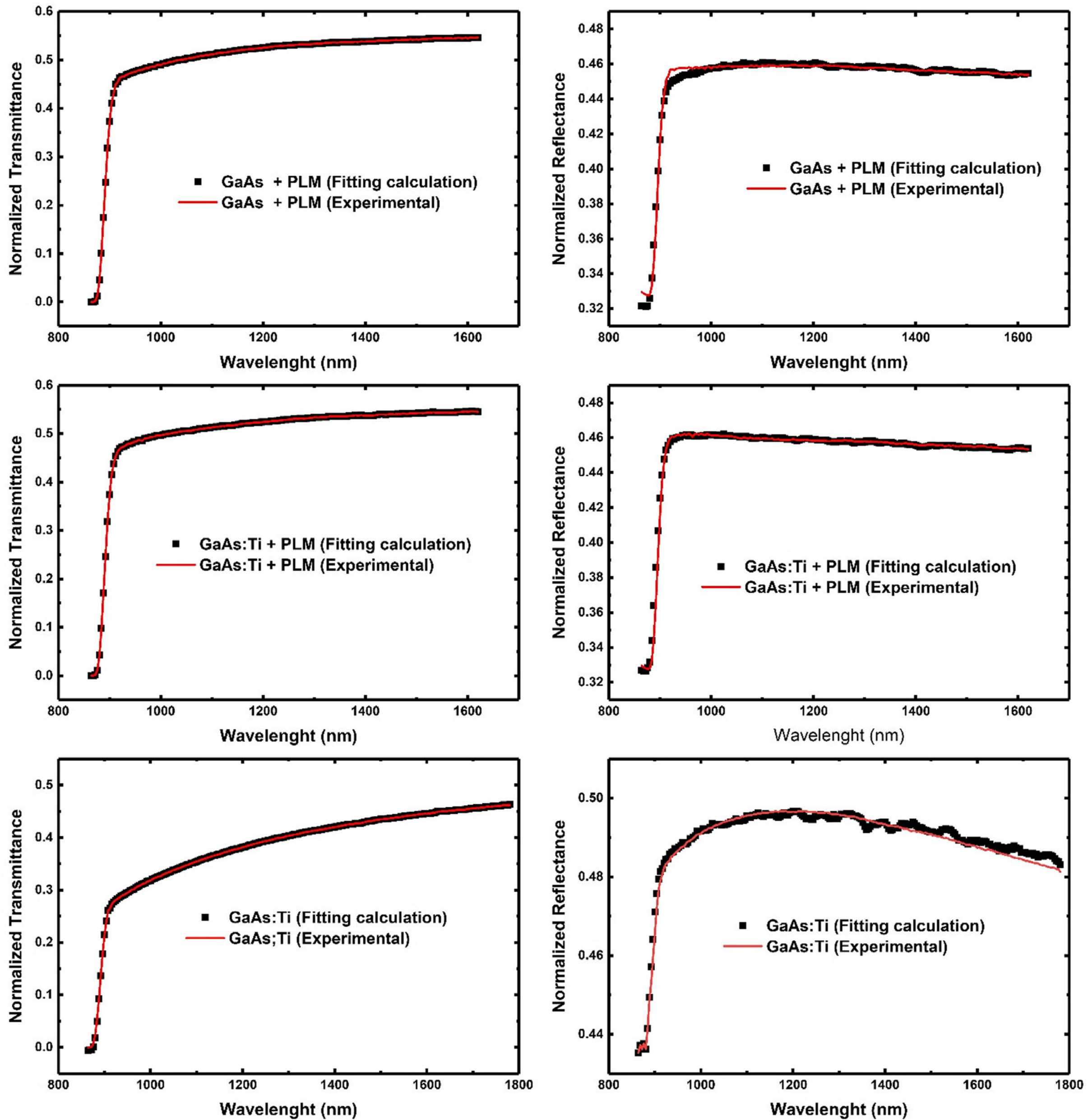

Figure 4. Experimental normalized transmittance and reflectance for a sample processed by PLM (GaAs + PLM), a sample implanted and subsequently processed by PLM (GaAs:Ti + PLM), and as-implanted GaAs:Ti. The resulting fitted curves obtained from Equation (5) and (6) are also shown.

implantation energy and divided by the amorphous layer thickness yields 1.4×10^{22} keV cm^{-3}, which fits within the amorphization range reported in ref. [15]. Therefore, we conclude that the observed sub-bandgap absorption in the GaAs:Ti sample (as implanted with no PLM treatment) is due to a full amorphization of the implanted layer.

For the GaAs:Ti + PLM sample, the regression parameter was $r = 0.991$ and the following values for the fitting parameters were obtained: $\text{Ln}A = -10.90 \pm 0.08\,\text{eV}^{-1}$ and $1/E_0 = 5.73 \pm 0.08\,\text{eV}^{-1}$, which yields $E_0 = 0.17$ eV. The GaAs + PLM sample was also fitted in the same range ($r = 0.988$, $E_0 = 0.13$ eV), although the exponential behavior is not so clear for this sample. The exponential behavior given by Equation (7) is characteristic of both amorphous GaAs and defective crystalline GaAs. For ion-implanted weakly damaged GaAs, an increase of E_0 is observed with increasing implantation dose, as long as the crystalline structure is preserved. The value decreases when amorphous regions are formed.[15–17] For defective crystalline GaAs resulting from laser irradiation with a Nd–glass laser ($\lambda = 530$ nm, 40 ns pulse), an increase of E_0 from 0.1 to 0.4 eV is observed as laser fluence increases from 0.56 to 0.93 J/cm^{-2}.[14] The observed absorption in these samples is attributed to the presence of point defects or clusters of point defects (vacancies, antisite defects, and vacancy–antisite

© 2024 The Authors. physica status solidi (a) applications and materials science published by Wiley-VCH GmbH

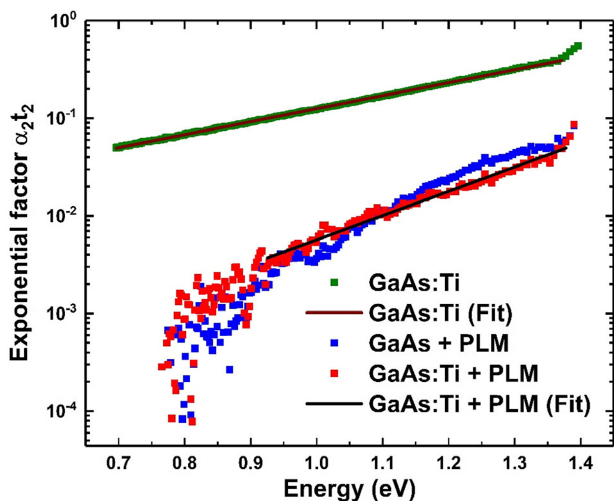

Figure 5. Absorption coefficient as a function of energy for a sample processed by PLM (GaAs + PLM), a sample implanted and subsequently processed by PLM (GaAs:Ti + PLM), and as-implanted GaAs:Ti sample.

complexes). These types of defects are also observed after thermal annealing treatment of the GaAs.[22] Our results with 0.5 J/cm^{-2} and 20 ns pulse duration (and therefore higher energy density per unit time) are consistent with the results reported by Wesch et al.[14] So, we suggest the same type of point defects or point defect clusters are responsible of the observed sub-bandgap absorption. In addition, the gap energy distribution of these defects was modeled by Zammit et al.[15] by the combination of an exponential valence-band tail distribution and a Gaussian distribution of gap states. The peak of the Gaussian distribution is related to the characteristic E_0 energy, which increases as the peak shifts away from the valence-band edge. Given the obtained low values of E_0, according to this model, the peak of the localized states in our samples would be very close to the valence band. The higher E_0 value for the GaAs:Ti + PLM sample would be consistent with a higher concentration of defects in this sample. Yet, the absorption coefficient values are very similar. The differences can also be attributed to the different nature of the samples: the GaAs + PLM sample is crystalline before the PLM process, while the GaAs:Ti + PLM is amorphous due to the implantation process prior to the PLM. Furthermore, the presence of a high Ti concentration would also affect the energy of the point defects present in the samples. Therefore, we conclude that the observed absorption in the PLM-processed samples is due to the formation of point defects induced by the PLM process and slightly modified by the Ti presence. So, the PLM processing could be used as a processing tool for enhancing sub-bandgap GaAs absorption. We also conclude that Ti supersaturation of GaAs does not produce any significant enhancement of its absorption properties beyond the effects of the PLM process.

Finally, to check our assumption that multiple reflections at the interface between layers 2 and 3 are negligible, we have computed the parameter $|r|^2_{23}$. For a wavelength $\lambda = 892$ nm, for which the maximum α_2 value is obtained ($\alpha_2 = 7.2 \times 10^3$ cm^{-3} for the GaAs:Ti + PLM sample). We obtain $|r|^2_{23} = 4.9 \times 10^{-5}$, which is indeed negligible compared to the reflectance at other interfaces (for instance, $|r|^2_{12} = 0.325$ at the same wavelength).

Table 1 shows the electrical parameters obtained at room temperature. All the samples are n-type according to the Hall effect measurements. The uncertainty in the measurements of the reference sample and the Ti-implanted samples is high because of the dispersion of the measured results at the different configurations. As expected, a very high sheet resistance and low carrier concentration (very close to the intrinsic value[23]) is obtained for the reference sample. After just the PLM process, a clear decrease of the mobility is observed, together with an increase of the carrier concentration of about one order of magnitude. These results are consistent with the previous conclusion of point defects being induced by the PLM process. These point defects would be responsible of the decrease of the mobility and, according to our electrical measurements, there is also some electrical activation of the point defects, increasing the electron concentration by one order of magnitude. The combined effect is a slight decrease of the sheet resistance, which remains in the 10^9 Ω range. Concerning the Ti-implanted and PLM-processed samples, the carrier concentration remains in the same order as in the just PLM-processed sample, but there is a further decrease of the mobility by a factor of 3, leading to an overall increase of sheet resistance. Clearly, there is no electrical activation of the implanted Ti and its only effect from the electrical point of view is to decrease the mobility. It is noted that the Ti supersaturation did not have effect in the sub-bandgap optical properties either. This is an unexpected result, since the theoretical calculations for the formation of an intermediate band in supersaturated GaAs:Ti are similar (and even more favorable) than for other materials, such as GaP:Ti,[2,12] for which the impurity activation is observed using the same processing techniques.[5] Conventional furnace annealing has not been tried because, as previously explained, supersaturated semiconductors are metastable materials, requiring out of equilibrium techniques for their fabrication, and the thermal annealing deactivates their properties.[24–26]

Figure 6 shows the calibrated spectral response of the samples. For the reference GaAs sample, the expected abrupt increase of the photo-response for energies above the direct bandgap ($\lambda < 880$ nm; h$\nu > 1.43$ eV) is observed. The values

Table 1. Electrical results obtained by Hall measurements under van der Pauw condition.

Parameters at room temperature [300 K]	GaAs reference	GaAs + PLM [0.50 J cm^{-2}]	GaAs:Ti + PLM [0.50 J cm^{-2}]
Carrier concentration [cm^{-3}]	$(7.0 \pm 0.5) \times 10^5$	$(9.5 \pm 0.9) \times 10^6$	$(9 \pm 4) \times 10^6$
Mobility [cm^{2}V^{-1}s^{-1}]	$(2.0 \pm 1.1) \times 10^3$	$(3.8 \pm 1.0) \times 10^2$	$(1.2 \pm 0.7) \times 10^2$
Sheet resistance [Ω]	$(4.4 \pm 2.4) \times 10^9$	$(1.7 \pm 0.5) \times 10^9$	$(5.5 \pm 1.0) \times 10^9$

© 2024 The Authors. physica status solidi (a) applications and materials science published by Wiley-VCH GmbH

18626319, 0, Downloaded from https://onlinelibrary.wiley.com/doi/10.1002/pssa.202400123 by Spanish Cochrane National Provision (Ministerio de Sanidad), Wiley Online Library on [21/11/2024]. See the Terms and Conditions (https://onlinelibrary.wiley.com/terms-and-conditions) on Wiley Online Library for rules of use; OA articles are governed by the applicable Creative Commons License

18626319, 0, Downloaded from https://onlinelibrary.wiley.com/doi/10.1002/pssa.202400123 by Spanish Cochrane National Provision (Ministerio de Sanidad), Wiley Online Library on [21/11/2024]. See the Terms and Conditions (https://onlinelibrary.wiley.com/terms-and-conditions) on Wiley Online Library for rules of use; OA articles are governed by the applicable Creative Commons License

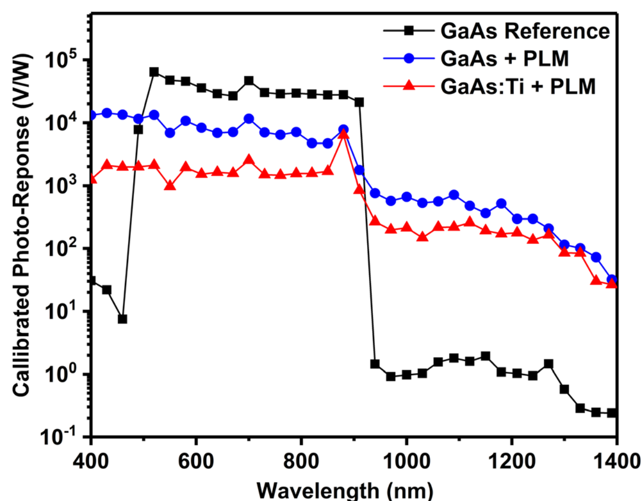

Figure 6. Photo-responsivity of GaAs reference, GaAs laser annealed at 0.50 J/cm^{-2}, and implanted and laser-annealed GaAs at 0.50 J/cm^{-2} fluence.

obtained for energies below the bandgap are in the noise level of the measurement. This is evidenced by the erratic behavior of the measured phase provided by the lock-in amplifier (the phase values are shown in Figure S6, Supporting Information). An abrupt decrease of the GaAs photo-response is observed for high energies, for the wavelengths below 500 nm, even though absorptance remains high in this range. We attribute this result to light being absorbed very close to the surface, owing to the increasing absorption coefficient, together with a high recombination rate at the surface. For the just PLM-processed sample, a very strong photo-response is observed in the below bandgap region (around 2×10^4 V W^{-1} in the 1200–880 nm range, which is nearly 1% of the GaAs reference above bandgap maximum value). The photo-response decreases as the wavelength increases, with a behavior very similar to the observed for the absorptance. A stable measurement of the signal phase is obtained from the lock-in amplifier, indicating a clear signal with respect to the noise level (shown in Figure S6, Supporting Information). We have not found any previous reported result of such significant sub-bandgap photo-response, at room temperature, induced by laser annealing. The PLM process does not only induce absorption, but also this absorption is converted into a very significant photoconductance, which could be used to extend the GaAs photosensitive region in the photoconductive devices.

For the Ti-implanted and PLM-processed sample, in the below bandgap region, a significant photo-response is also observed, with a lower value than the observed in the just PLM-processed sample. Again, this lower signal can be related to lower mobility. We conclude the response is not related to the incorporation of Ti, and the presence of Ti does not enhance this signal.

It is also observed that the above bandgap signal of the samples processed by PLM does not show the abrupt decrease at the lowest wavenumbers observed for the GaAs reference sample. This result could be related to a passivation effect of the PLM process, probably related to the oxide layer formed after the laser annealing, leading to a decrease of the surface recombination rate. Such passivation effect has been reported for Ti-supersaturated GaP processed by PLM[27] in air and attributed to an oxide layer composed of Ga, P, and O with a Ga/P ratio lower than 1. It has also been reported that the oxidation state of Ga plays a critical role on the density of defects and Fermi level pinning at GaAs and InGaAs interfaces, being the Ga 3+ oxidation state (corresponding to a Ga_2O_3 passivation layer) responsible of high interfacial defect density,[28] while the presence of Ga_2O was not related to any Fermi level pinning. Passivation of GaAs by Ga_2O has also been reported.[29] According to these results, a passivating effect of the PLM process could be related to changes in the oxidation states of the Ga present in the native oxide of the GaAs.

The immediate explanation of the observed photo-response is that it is directly related to the sub-bandgap absorption previously shown, and that the point defects induced by the nanosecond PLM process are responsible for the photo-response. The PLM process melts the top layer, and the GaAs recrystallizes from the crystalline seed underneath. The recrystallization process occurs during liquid/solid epitaxy phase which introduces point defects on the processed layer. The broad spectrum of the photo-response reflects the convolution of the initial and final densities of states between which the electronic transitions responsible for the sub-bandgap absorption take place. As previously discussed, the energy distribution of the defects within the bandgap is not expected to be a single level, but a combination of different distributions, leading to multiple possible energy transitions. It is also noted that the transitions can reach empty extended states in the conduction band.

3. Conclusion

In this work, double-sided polished, semi-insulating GaAs was implanted with Ti with a dose of 2×10^{15} cm^{-2} and subsequently processed by PLM, at specific fluence of 0.50 J/cm^{-2}. Electrical and optical analyses were conducted on the resulting material. The electrical results show no electrical activation of the Ti-implanted samples. However, a significant decrease of mobility and a slight increase of the carrier concentration was obtained for the PLM-processed samples (implanted and without Ti implantation). Optical results show a significant absorption below the bandgap, about 6.5%. Furthermore, sub-bandgap GaAs photoresponsivity can be detected in the processed samples. The just PLM samples also demonstrate sub-bandgap photo-response and absorption. The fabricated samples were able to demonstrate the ability to detect photons below the bandgap of the reference material, which is the first step toward fabricating a near-infrared photodetector using such material.

4. Experimental Section

Semi-insulating GaAs grown in the <100> direction, double-sided polished, 325 μm of thickness with a resistivity of 5.3×10^7 Ω cm at room temperature and mobility of 4000 cm^2 V^{-1}s^{-1} (as given by the manufacturer) was implanted in a refurbished VARIAN CF3000 ion implanter by the polished surface with a $^{48}Ti^+$ dose of 2×10^{15} cm^{-2} at energy of 32 keV. The implantation was conducted using a 7° tilt angle, to reduce

© 2024 The Authors. physica status solidi (a) applications and materials science published by Wiley-VCH GmbH

channeling.[30] The implanted wafer then was cut into 2 × 1 cm rectangular samples.

A set of samples were irradiated with an ArF^+ excimer pulsed laser in ambient air ($\lambda = 193$ nm, with a pulse duration of 20 ns full width at half maximum). The laser annealing fluence used was 0.50 J/cm^{-2}. The laser beam was homogenized in a square spot area of 1 × 1 mm^2 on the sample surface. The 1 × 2 cm sample area was processed by overlapping single pulses across the irradiation plane. The overlapping between consecutive horizontal and vertical irradiated areas was 5 and 10 μm, respectively. The samples were prepared with just PLM-processed un-implanted GaAs, as well as implanted samples.

The implanted dose and PLM fluence were chosen to obtain a sufficiently thick supersaturated GaAs:Ti layer with good crystalline quality, according to previous results.[13] Higher Ti concentrations were avoided to prevent the destabilization of the plane-front solidification during the PLM process leading to the cellular breakdown effect.[31]

A single-sided polished, undoped semi-insulating <100 > GaAs wafers, with 350 μm of thickness was used for analyzing the crystal quality of the implanted samples, cross-section transmission electron microscopy (TEM) was used. Lamellae from a reference substrate, an as-implanted reference, a just PLM-processed sample, and a Ti-implanted and PLM-processed samples were extracted using focused-ion-beam scanning electron microscopy, with a Helios Nanolab 650 model. The structure was analyzed by obtaining TEM images in a JEOL JEM 3000 F microscope operating at 300 kV.

For optical characterization of the recrystallized layer, transmittance $T(\lambda)$ and reflectance $R(\lambda)$ (in specular mode) spectra in the range of 400–1780 nm were obtained using a ultraviolet–visible–near-infrared (UV–vis–NIR) PerkinElmer Lambda 1050 spectrometer. The results were used to obtain the absorption coefficient using the incoherent limit for the T and R equations, as described later.[19]

The measured transmittance and reflectance data were normalized to correct calibration inaccuracies of the measurements, so that T + R equaled 100% in the region where no absorption took place. For the normalization, a correction factor for the T and R measurements was calculated as the mean value of the ratio of the measured T or R with respect to known T or R data in the 1600–1800 nm range. The whole spectrum was then divided by this factor. The reference T and R data for this correction were obtained using the refractive index values from the Sellmeier dispersion formula given by Skauli et al.[20] and assuming the incoherent limit for the multiple reflections on the backside of the substrate, due to its 325 μm thickness.[19] These calculated T and R values were equal to the obtained ones using the reflectance calculator provided by Film Metrics in its website,[32] setting and air/GaAs (325 μm)/air system with a 4 nm data point spacing, corresponding to our measurements resolution. For the as-implanted sample, for which absorption was observed over the whole measured range, a mean value of the correction factors of the other samples was used.

After the laser melting process, some of the samples were prepared for characterization with the van der Pauw setup. The samples were cut into 0.5 × 0.5 cm^2. Triangular metal contacts were deposited on the corners of the samples by Joule evaporation of an Au:Ge (88:12 ratio) layer of 100 nm, and subsequently an e-beam evaporation of a 200 nm Au layer, without breaking the vacuum. Supersaturated semiconductors obtained using nonequilibrium techniques are known to be metastable materials. Deactivation of the sub-bandgap absorption properties was reported after thermal equilibrium annealing.[24–26] Therefore, no annealing was performed on the contacts after evaporation. It is noted, however, that the van der Pauw setup used for the electrical and optoelectronic characterization avoided the influence of contact resistance. The recipe used for the contacts can be found in the literature.[33,34]

The van der Pauw configuration was used to perform two different types of measurements. First, the sheet resistance of the samples was measured in darkness at room temperature using a Keithley 4200 SCS equipped with four source and measure units. Four configurations for current injection and measured voltage were used, with positive and negative current for each configuration. The sheet resistance was obtained as the mean value. The mobility and carrier concentration were also obtained by Hall effect measurements using four configurations, positive and negative magnetic field (0.9 T) and positive and negative current. Results are obtained as the mean value of the 16 configurations to avoid undesired thermogalvanometric effects.

Second, the spectral sheet photoconductance of the samples was measured. A Keithley 2636 current source was configured to feed 10 nA between two of the contacts. A simple schematic diagram of the measurement setup and the samples geometries can be found in Figure S1 and S2, Supporting Information, respectively. The AC-photogenerated voltage was obtained with a Stanford SR-830 DSP dual-phase lock-in amplifier. However, due to the high resistivity of the samples, an INA111AP instrumentation amplifier was used to increase the input impedance of the lock-in amplifier. A UV–vis–NIR Horiba IHR320 monochromator with a 250 W tungsten halogen lamp was used as a light source. A chopper was configured to produce AC illumination at 23 Hz. Finally, the spectral power density of the light impinging on the sample was measured with a calibrated Si S2281 Hamamatsu photodiode in photovoltaic mode. All the samples measured were injected with a constant 10 nA current. The following equation shows the basic parameters of interest:

$$R_{(\text{sample})}(\lambda) = \frac{V_{(\text{sample})}(\lambda)}{P(\lambda)\, x A_{(\text{sample})}} \tag{8}$$

$$P(\lambda) = \frac{V_{(\text{sensor})}(\lambda)}{R_{(\text{sensor})}(\lambda)\, x A_{(\text{sensor})}} \tag{9}$$

where $R_{(\text{sample})}(\lambda)$ and $R_{(\text{sensor})}(\lambda)$ are the measured responsivity as a function of wavelength of the sample and the detector, respectively; $V_{(\text{sample})}(\lambda)$ and $V_{(\text{sensor})}(\lambda)$ are the measured voltage produced by the light illumination and measured by the lock-in of the sample and the detector as a function of the wavelength, respectively; $P(\lambda)$ is the incident optical power density; and $A_{(\text{sample})}$ and $A_{(\text{sensor})}$ are the area of the sample and detector, respectively. $R_{(\text{sensor})}(\lambda)$ is given by the manufacturer of the reference photodiode, while $A_{(\text{sensor})}$ is 0.785 cm^2. The power density spectra of the light source can be found in Figure S3, Supporting Information.

Supporting Information

Supporting Information is available from the Wiley Online Library or from the author.

Acknowledgements

The authors would like to acknowledge the "CAI de Técnicas Físicas" of the Universidad Complutense de Madrid for the fabrication processes. Authors also acknowledge Servicio de Nanotecnología y Análisis de Superficies del CACTI de la Universidad de Vigo for ToF–SIMS measurements. The authors acknowledge the use of instrumentation as well as the technical advice provided by the National Facility ELECMI ICTS, node "Laboratorio de Microscopías Avanzadas" at University of Zaragoza and ICTS–CNM from Madrid for the TEM images. This work was partially supported by the Spanish Research Agency (AEI, Ministry of Research and Innovation) and the European Regional Development Fund (ERDF) under grant nos. PID2020-116508RB-I00 and PID2020-117498RB-I00. The authors also acknowledge financial support via research grants HyperSolar (TED2021-130894B-C21/C22) funded by the Recovery and Resilience Facility of the EU. D. Caudevilla would also acknowledge the grant no. PRE2018-083798, financed by MICINN and European Social Fund. F. Pérez-Zenteno is also thankful for financial collaboration from the Mexican grants program CONACyT and for predoctoral contract from UCM (call CT58/21-CT59/21). The authors would also like to acknowledge financial support from the Ministry of Education in the Kingdom of Saudi Arabia. G. Godoy-Pérez and R. Benítez-Fernández acknowledge the research contracts under the Investigo Program (grant nos. CT19/23-INVM-35 and CT19/23-INVM-27) of the Ministerio de Trabajo y Economía Social.

© 2024 The Authors. physica status solidi (a) applications and materials science published by Wiley-VCH GmbH

18626319, 0, Downloaded from https://onlinelibrary.wiley.com/doi/10.1002/pssa.202400123 by Spanish Cochrane National Provision (Ministerio de Sanidad), Wiley Online Library on [21/11/2024]. See the Terms and Conditions (https://onlinelibrary.wiley.com/terms-and-conditions) on Wiley Online Library for rules of use; OA articles are governed by the applicable Creative Commons License

Conflict of Interest

The authors declare no conflict of interest.

Data Availability Statement

The data that support the findings of this study are available from the corresponding author upon reasonable request.

Keywords

excimer laser processings, gallium arsenide, ion implantations, supersaturated semiconductors

Received: January 30, 2024
Revised: March 25, 2024
Published online:

[1] A. Luque, A. Martí, *Phys. Rev. Lett.* **1997**, *78*, 5014.
[2] P. Palacios, P. Wahnón, S. Pizzinato, J. C. Conesa, *J. Chem. Phys.* **2006**, *124*, 014711.
[3] A. Luque, A. Martí, E. Antolín, C. Tablero, *Phys. B* **2006**, *382*, 320.
[4] J. P. Mailoa, A. J. Akey, C. B. Simmons, D. Hutchinson, J. Mathews, J. T. Sullivan, D. Recht, M. T. Winkler, J. S. Williams, J. M. Warrender, P. D. Persans, *Nat. Commun.* **2014**, *5*, 1.
[5] J. Olea, A. del Prado, E. García-Hemme, R. García-Hernansanz, D. Montero, G. González-Díaz, J. Gonzalo, J. Siegel, E. López, *Prog. Photovolt.: Res. Appl.* **2018**, *26*, 214.
[6] H. H. Gandhi, D. Pastor, T. T. Tran, S. Kalchmair, L. A. Smilie, J. P. Mailoa, R. Milazzo, E. Napolitani, M. Loncar, J. S. Williams, M. J. Aziz, *Phys. Rev. Appl.* **2020**, *14*, 064051.
[7] M. L. Lee, F. W. Huang, P. C. Chen, J. K. Sheu, *Sci. Rep.* **2018**, *8*, 1.
[8] S. Sonoda, *Appl. Phys. Lett.* **2012**, *100*, 202101.
[9] G. Garcia, P. Sanchez-Palencia, P. Palacios, P. Wahnon, *Nanomaterials* **2020**, *10*, 283.
[10] S. Kumar, G. B. Corrêa Jr, C. Devi, D. Jacobsson, A. Johannes, C. Ronning, W. Paraguassu, W. Paschoal Jr, H. Pettersson, *Nanotechnology* **2020**, *31*, 205705.
[11] A. V. Kudrin, V. P. Lesnikov, Y. A. Danilov, M. V. Dorokhin, O. V. Vikhrova, P. B. Demina, D. A. Pavlov, Y. V. Usov, V. E. Milin, Y. M. Kuznetsov, R. N. Kriukov, *Semicond. Sci. Technol.* **2020**, *35*, 125032.
[12] P. Wahnón, C. Tablero, *Phys. Rev. B* **2002**, *65*, 165115.
[13] S. Algaidy, D. Caudevilla, F. Perez-Zenteno, R. García-Hernansanz, E. García-Hemme, J. Olea, E. San Andrés, S. Duarte-Cano, J. Siegel, J. Gonzalo, D. Pastor, A. del Prado, *Mater. Sci. Semicond. Process.* **2023**, *153*, 107191.
[14] W. Wesch, E. Wendler, G. Götz, K. Unger, H. Röppischer, C. Resagk, *Phys. Status Solidi B* **1985**, *130*, 539.
[15] U. Zammit, M. Marinelli, R. Pizzoferrato, F. Mercuri, *Phys. Rev. B* **1992**, *46*, 7515.
[16] E. Wendler, W. Wesch, *Nucl. Instrum. Methods Phys. Res. B: Beam Interact. Mater. Atoms* **1993**, *73*, 489.
[17] S. Creutzburg, E. Schmidt, P. Kutza, R. Loetzsch, I. Uschmann, A. Undisz, M. Rettenmayr, F. Gala, G. Zollo, A. Boulle, A. Debelle, *Phys. Rev. B* **2019**, *99*, 245205.
[18] W. Wesch, E. Wendler, G. Götz, *Nucl. Instrum. Methods Phys. Res. B: Beam Interact. Mater. Atoms* **1987**, *22*, 532.
[19] N. Maley, *Phys. Rev. B* **1992**, *46*, 2078.
[20] T. Skauli, P. S. Kuo, K. L. Vodopyanov, T. J. Pinguet, O. Levi, L. A. Eyres, J. S. Harris, M. M. Fejer, B. Gerard, L. Becouarn, E. Lallier, *J. Appl. Phys.* **2003**, *94*, 6447.
[21] J. Olea, A. Del Prado, D. Pastor, I. Mártil, G. González-Díaz, *J. Appl. Phys.* **2011**, *109*, 113541.
[22] R. C. Roca, K. Fukui, H. Mizuno, M. Suzuki, I. Kamiya, *Phys. Status Solidi B* **2020**, *257*, 1900391.
[23] J. Olea, G. González-Díaz, D. Pastor, I. Mártil, A. Martí, E. Antolín, A. Luque, *J. Appl. Phys.* **2011**, *109*, 063718.
[24] B. K. Newman, E. Ertekin, J. T. Sullivan, M. T. Winkler, M. A. Marcus, S. C. Fakra, M. J. Sher, E. Mazur, J. C. Grossman, T. Buonassisi, *J. Appl. Phys.* **2013**, *114*, 133507.
[25] C. B. Simmons, A. J. Akey, J. J. Krich, J. T. Sullivan, D. Recht, M. J. Aziz, T. Buonassisi, *J. Appl. Phys.* **2013**, *114*, 243514.
[26] M. Wang, R. Hübner, C. Xu, Y. Xie, Y. Berencén, R. Heller, L. Rebohle, M. Helm, S. Prucnal, S. Zhou, *Phys. Rev. Mater.* **2019**, *3*, 044606.
[27] J. Olea, S. Algaidy, A. del Prado, E. Garcia-Hemme, R. Garcia-Hernansanz, D. Montero, D. Caudevilla, G. Gonzalez-Diaz, E. Soria, J. Gonzalo, *J. Alloys Compd.* **2020**, *820*, 153358.
[28] C. L. Hinkle, M. Milojevic, B. Brennan, A. M. Sonnet, F. S. Aguirre-Tostado, G. J. Hughes, E. M. Vogel, R. M. Wallace, *Appl. Phys. Lett.* **2009**, *94*, 162101.
[29] M. J. Hale, S. I. Yi, J. Z. Sexton, A. C. Kummel, M. Passlack, *J. Chem. Phys.* **2003**, *119*, 6719.
[30] B. Clerjaud, *J. Phys. C: Solid State Phys.* **1985**, *18*, 3615.
[31] J. M. Warrender, J. Mathews, D. Recht, M. Smith, S. Gradečak, M. J. Aziz, *J. Appl. Phys.* **2014**, *115*, 163516.
[32] https://www.filmetrics.com/reflectance-calculator (accessed: 1 December 2022).
[33] R. H. Cox, H. Strack, *Solid-State Electron.* **1967**, *10*, 1213.
[34] A. Piotrowska, *Acta Phys. Pol. A* **1993**, *84*, 491.

© 2024 The Authors. physica status solidi (a) applications and materials science published by Wiley-VCH GmbH

18626319, 0, Downloaded from https://onlinelibrary.wiley.com/doi/10.1002/pssa.202400123 by Spanish Cochrane National Provision (Ministerio de Sanidad), Wiley Online Library on [21/11/2024]. See the Terms and Conditions (https://onlinelibrary.wiley.com/terms-and-conditions) on Wiley Online Library for rules of use; OA articles are governed by the applicable Creative Commons License